UM-P-92/73

Paper presented at the Third International Conference on Nuclear Microprobe Technology and Applications, Uppsala, Sweden, June 1992.

Microprobe Channeling Analysis of Pyrite Crystals.

D.N. Jamieson[1] and C.G. Ryan[2]

[1] Microanalytical Research Centre, School of Physics, University of Melbourne, Parkville, VIC 3052, Australia.

[2] CSIRO, Heavy Ion Analytical Facility, Division of Exploration Geoscience, P.O. Box 136, North Ryde NSW 2113, Australia.

Abstract

Nuclear microprobe analysis has provided much useful information about the composition of microscopic inclusions in minerals, mainly through the use of Particle Induced X-ray Emission (PIXE). However this technique, while powerful, does not provide any direct information about the chemical state, in particular the lattice location, of the elements in the mineral. This information is often of crucial importance in understanding the ore genesis. The technique of ion channeling may be used to identify lattice location, but many minerals occur as microscopic crystals. Therefore it is necessary to utilise a nuclear microprobe with the technique of Channeling Contrast Microscopy (CCM). As many minerals contain interesting trace elements, it is necessary to measure both the yield of backscattered particles and the induced x-rays to get a clear picture of the lattice location of the elements in the crystal. CCM with PIXE was used to analyse natural pyrite crystals containing a variety of substitutional and non-substitutional elements and natural pyrite crystals from a gold bearing ore. In the latter case, evidence was obtained for two habits for Au in the 400 μm crystals: one as inclusions of Au rich minerals, the other substituted on the pyrite lattice sites.

INTRODUCTION

The use of focused MeV ion beams for the analysis of geological materials is now very well established [1-3]. The results of this work have provided useful information about trace element concentrations in a variety of minerals leading to 1) a geothermometer based on trace Ni in garnet [4], 2) knowledge of the structure and metasomatic processes which occur in the upper mantle

[5–8], 3) trace element signatures which distinguish diamondiferous and barren kimberlites and lamporites [9–11] and many other applications.

Most of these applications have involved the use of Proton Induced X-ray Emission (PIXE) [12] and have exploited the excellent trace element sensitivity of that technique. The specimens typically consisted of polycrystalline assemblages which contain micron-sized inclusions. However, little work has been done on channeling the ion beam into the crystal despite the useful information that can be obtained. This is usually because the crystals are too small, or non-uniform, for analysis with unfocused beams. A notable exception is the work of Sellschop who has made extensive channeling analyses to investigate the properties of diamonds [13].

The method of ion channeling analysis [14], originally used to study synthetic crystals, is applicable to the study of trace elements in minerals, provided a microprobe is employed. For example, experience in the investigation of synthetic polycrystalline $Y_1Ba_2Cu_3O_{7-\delta}$, an analogue of the study of natural systems, showed how Channeling Contrast Microscopy (CCM) [15] and PIXE could be combined to identify the lattice site of a trace element, in this case Fe [16]. In the case of minerals, knowledge of the lattice sites of trace elements is important because it leads to the understanding of the mineral growth mechanisms. In the present work, we apply the combined PIXE and CCM technique to the study of Au in natural pyrite crystals from the Emperor gold-telluride deposit in Fiji.

The high As levels observed in natural pyrite systems, including those of the Emperor deposit, show dynamical growth features such as pronounced zoning. This has been interpreted as disequilibrium deposition of a metastable high As pyrite phase [17,18]. Such a phase may host precious metals such as the gold in pyrite. Alternatively, other workers have developed models involving the adsorption and reduction of Au complexes on the surface of pyrite [19,20] that lead to the conclusion that Au nucleates at electrically active sites on the pyrite to form discrete Au metal grains [20, 21]. Direct determination of the residence of Au in pyrite would be very useful in furthering an understanding of these processes.

The combined use of PIXE imaging and CCM provides a tool for studying the incorporation of gold in pyrite. The sensitivity of PIXE using the nuclear microprobe enables trace distributions of Au to be distinguished from discrete gold minerals. Targeting areas showing trace Au, CCM

then provides a means to determine if this gold is in the pyrite lattice. Studies like this of the details of incorporation of gold in ores are essential to furthering the understanding of the genesis of hydrothermal gold deposits and are important for the development of improved beneficiation methods in ore processing.

SAMPLES

To demonstrate the feasibility of channeling into specific crystallographic axes and to assess natural pyrite crystal quality, measured by ion channeling, a selection of natural euhedral pyrite crystals were analysed in addition to the Au bearing Emperor pyrite.

The first type was in the form of 1 cm cubes displaying (100) faces marked by the characteristic striation pattern of such cubes [22]. Optical microscopic examination of a cleaved crystal revealed a dense mosaic structure of with a characteristic scale of 10 μm. Laue x-ray diffraction patterns confirmed the <100> orientation of the crystal.

The second type were cut from a crystalline assemblage of trucated octohedra. The cut was made parallel to a clearly identifiable 1 mm triangular (111) planar face [22] so that the sample could be mounted with a <111> axis in close alignment with the analysis beam.

The third type of crystal was obtained directly from a quartz-pyrite vein of the Emperor gold deposit in Fiji [23]. A sample of the vein was crushed and a pyritohedral crystal displaying 400 μm pentagonal faces was selected on the basis of best flatness of the faces and degree of symmetry of the crystal. This size was typical of the crystals in the vein. In pyritohedral crystals, the <210> axis is normal to the pentagonal faces [22]. Representative samples of other crystals from the same region had shown, by prior PIXE analysis, to contain up to 0.4 % Au [23, 24].

Preliminary measurements with Backscattering Spectrometry (BS) on each sample revealed evidence for a surface coating of light elements which could potentially degrade channeling measurements. Therefore, prior to channeling analysis, the crystals were subjected to a 5 minute etch in a bath of concentrated HNO_3/HF held at 50° to remove any surface contamination. This etch also removed a small amount of material from the surface of the crystals. This was beneficial since the surface crystal could have been damaged during exposure to hostile environments.

EXPERIMENT

Images of the crystals were obtained using both 3 MeV H^+ to examine the trace element composition

as well as 2 MeV He^+ to measure the crystal quality, χ_{min}. The images were obtained using the Melbourne Nuclear Microprobe with the beam focused to a 5 μm spot and typically scanned over 1×1 mm^2 regions of the crystals. The x-ray detector was located at 135° and was fitted with x-ray absorbers of 100 μm Be or 240 μm Al. Backscattered particles were detected by a surface barrier detector located at 150° or 154°.

RESULTS

1) <100> pyrite crystal.

Images from BS and PIXE revealed numerous inclusions from 200 μm down to ~10 μm in size composed of compounds of Fe, Ca, F, O, Si and S with traces of Ni and Ti. The pyrite matrix itself surrounding these inclusions had an excellent crystal quality with a very low χ_{min}. This is shown by the spectra in figure 1 which were extracted from those regions of the sample that were free from inclusions larger than 10 μm in size. These spectra show that the χ_{min} for the <100> axis was 3.3 % which compares favourably with values of ~2 % for high quality synthetic Si crystals.

The angular yield curves for the <100> axis also confirm the quality of the crystal. The curves, shown in figure 2, and summarised in table 1, show that the angular half widths, $\psi_{\frac{1}{2}}$, are characteristic of good crystal. The angular yield curve for Fe from 2 MeV He^+ is distorted because of a small misalignment between the tilt plane and the <100> axis, and also because the tilt moved a small number of Fe rich inclusions under the beam. A signal from these inclusions can be seen at the surface energy of Fe in the spectrum from the randomly oriented crystal in figure 1.

Images of the inclusions present in the crystal are shown in the in the BS and PIXE CCM images in figure 3. Although the inclusions show up clearly in the PIXE images, the BS spectrum from the inclusions, extracted from the BS images shown for the randomly oriented crystal, were used to determine the stoichiometry. This was because the inclusions contain significant amounts of light elements with low energy x-rays that were absorbed by the x-ray filters. The images reveal three categories of inclusions:

1) 50–200 μm sized inclusions, irregularly shaped, in the stoichiometry of CaF_2.

2) 10–50 μm elongated inclusions in the stoichiometry of $Fe_1Si_4O_{12}$. These inclusions display the interesting property that the long axis of the inclusion is aligned with either a <100>, <110> or <111> axis. Other regions of this sample displayed even denser arrays of these inclusions.

3) 10-20 μm circular inclusions mainly composed of Ca and S. The small size and relative rarety prevented accurate compositional analysis. However these inclusions show up as minima in the images for the randomly aligned crystal and maxima in images of the aligned crystal showing that they contain less S than pyrite and are not aligned with the host crystal.

Figure 3 shows a significant improvement in the signal to noise ratio in the images of the inclusions obtained when the crystal was in the aligned orientation compared to the random orientation. This is because in the aligned orientation the large signal from the host crystal is significantly reduced, the precise amount depends on the quality of the crystal and the imaging method. This demonstrates the advantage of imaging unaligned inclusions while the host crystal in the aligned orientation.

The 3 MeV H^+ PIXE spectra (not shown) reveal the presence of Ni as a trace element but with a yield too small to produce images. However, the signal was sufficient to calculate a χ_{min} and angular scan which showed that the Ni was 100 % substitutional in the pyrite lattice, since the yield for the aligned crystal dropped to that of the Fe K_α, see figure 2. This result illustrates the utility of the combined PIXE/CCM technique for measurement of the lattice location of trace elements.

2) <111> crystal.

The 1 mm triangular face of the <111> oriented pyrite crystal displays excellent channeling, as can be seen from the spectrum for the randomly oriented crystal and aligned crystal shown in figure 4. The χ_{min} is 2.4 %, comparable to the <100> oriented crystal. The PIXE spectrum from the aligned crystal reveals traces of K, however the K signal in the PIXE spectrum for the randomly aligned crystal was swamped by background. Once again, this indicates the utility of crystal PIXE analysis from aligned crystals as a way of decreasing background in order to increase sensitivity to trace elements.

3) <210> crystal.

The results from the previous two crystals show that excellent channeling is possible in naturally occcuring pyrite crystals. In addition, the lattice location of trace elements can be determined. However, the pyritohedral crystals of the present study provide a much greater challenge for analysis by this technique. This is because the crystals themselves are small (400 μm) and heavily doped with As. The As is likely to perturb the crystal lattice t. degrade the crystal quality for channeling.

Further, the relatively high order of the normal axis makes the angular width of the channel relatively narrow and therefore more sensitive to imperfections. Theoretical calculations show that the <210> axis has a $\psi_{1/2}$ of 0.3° compared to 0.5° for the <100> axis [25]. The present crystals also display exfoliation of the surface, perhaps indicative of weathering, which would further degrade the channeling process. The acid etch, described above, removed some of the exfoliation to expose fresh crystal, however, despite the acid etch, the surface of the crystal retained a rough appearance. Despite these difficulties, it was found possible to channel into the <210> axis of the pyritohedron and a channeling spectrum is shown in figure 5. The channeling spectrum shows that the crystallinity was not as good as that of the former samples, with a χ_{min} of 24 % for Fe on the surface. This is larger than expected even given the relatively high order of the channel where a χ_{min} of around 9 % is expected [25]. The spectrum from the randomly oriented crystal shows the effect of the uneven surface topography of the crystal, since the yield apparently increases with depth faster than expected, showing that some particles backscatter from relatively shallow depths but recoil through a raised surface feature causing the particles to loose too much energy and thus appear at lower energies in the spectrum.

We believe that the surface topography does not significantly influence the χ_{min} in this case because the crystal was tilted by a small angle (~2°) from the aligned orientation to produce the spectrum for the randomly oriented crystal. This was satisfactory given the small $\psi_{\frac{1}{2}}$ of the <210> axis of 0.3° [25].

The most important result is that the channeling spectrum shows a degree of gold substitutionality. Owing to the relatively poor statistics in the gold plateau in the channeling spectrum it is not possible to determine an accurate value of the gold χ_{min} but the results are consistent with a value of at least 50 %. This suggests that at least 50 % of the Au is substitutional, at least in the surface ~500 nm probed by our 2 MeV He^+ analysis beam. Notice that the χ_{min} obtained for Au from PIXE was greater than 50 %, indeed it was 100 % within errors, owing to the relatively deep mean production depth where extensive dechanneling occurs in this poor crystal. It is interesting to note that the results for As are similar to those for Au (see table 3).

DISCUSSION

The channeling results can be used to clarify proposed mechanisms for the incorporation of Au

in pyrite. Phase equilibria in the Fe-As-S system argue for a maximum equilibrium concentration of As in pyrite of 0.5 wt% at 500°C [26]. Yet in natural systems, such as our <210> crystal, As concentrations of 8.9 wt% have been observed [18, 27]. This has been interpreted as the deposition of a metastable arsenian pyrite phase [27]. Studies of high As pyrite using TEM has shown evidence for 10 Å lamellae in the pyrite with a marcasite structure [27]. Such a layer may be the site of the incorporation of precious metals such as gold in pyrite. Arsenopyrite has a marcasite structure, so the common correlation of Au with As in hydrothermal systems may be partly a result of disequilibrium deposition of arsenopyrite. These growth features may also provide a site for a number of other elements, such as Cu and Se, seen to correlate with As [18].

There has been much interest in surface deposition processes to understand the genesis of hydrothermal gold ores. Experimental work by Jean and Bancroft [19] showed that gold can be deposited on pyrite surfaces. They proposed a two step process of adsorption of $AuCl_4^-$ complexes followed by reduction to Au on the semi-conducting pyrite surface. The presence of acceptors such as As in the pyrite, p-type semiconductor, aids in the reduction [20]. In low temperature systems the transport of gold is dominated by the $Au(HS)_2^-$ complex [28], and gold deposition probably involves the reduction of this species.

Starling et al. argued on textural grounds for the deposition of gold and tellurides on certain nucleation points on the surfaces of pyrite crystals [20]. They, and Knipe et al. [21], observed native gold and altaite (PbTe) on crystal edges, grain junctions, growth terraces and hydrothermal etch-pits, and argued that these sites represent electrically active sites for the reduction of Au complexes. To explain the connection between the experimentally observed uniform plating of gold [19] and the natural discrete nucleated gold grains, Bancroft and Hyland [29] have proposed that the adsorbed atoms diffuse across the sulfide surface to an active site. The high conductivity of gold ensures the transmission of the electronic characteristics of the site to the gold surface facilitating continued epitaxial growth. This mechanism, aided by geological time-scales, would suggest that little gold would be distributed throughout the pyrite. Instead it would be concentrated in discrete grains of gold and gold minerals.

The present results support the epitaxial growth model. Not only are the electronic characteristics of the nucleation site transmitted to the surface, but the crystal structure information is transmitted

as well. However, PIXE elemental maps of crystals from the same ore vein as the <210> crystal, originally located within 1 cm, reveal two habits for the Au [30]. One is conceatrated grains ~20 μm in size, that are probably Au metal and the other as a uniform low concentration Au distribution in the whole crystal. We believe that the present results are consistent with this; the substitutional Au is the uniform distribution and the non-substitutional Au is in the Au grains.

CONCLUSION

The technique of CCM has been combined with PIXE to provide information about the lattice location of trace elements in pyrite crystals. Naturally occuring crystals were found to be of excellent crystallinity, as measured by ion channeling. Evidence was also obtained for 50 % Au substitutionalty in pyrite crystals that contain both Au and As.

REFERENCES

[1] S.H. Sie, W.L. Griffin, C.G. Ryan, G.F. Suter and D.R. Cousens, Nucl. Instr. Meth. B54 (1991) 284.

[2] S.H. Sie, PIXE-6 conf.

[3] C.G. Ryan and W.L. Griffin, these proceedings.

[4] W.L. Griffin, D.R. Cousens, S.H. Sie and G.F. Suter, Contrib. Mineral. Petrol., 103 (1989) 109.

[5] D. Smith, W.L. Griffin, C.G. Ryan and S.H. Sie, Contrib. Mineral. Petrol. 107 (1991) 60.

[6] S.Y. O'Reilly, W.L. Griffin and C.G. Ryan, Contrib. Mineral. Petrol. 109 (1991) 98.

[7] W.L. Griffin, J.J. Gurney and C.G. Ryan, Contrib. Mineral. Petrol. 110 (1992) 1.

[8] W.L. Griffin, C.G. Ryan and D.J. Schulze, Proc. Fifth Int. Kimberlite Conf., Araxá, Brazil (1991) in press.

[9] W.L. Griffin, C.G. Ryan, S.Y. O'Reilly, P.H. Nixon and T.T. Win, ibid.

[10] W.L. Griffin, C.G. Ryan, J.J. Gurney, N.V. Sobolev and T.T. Win, ibid.

[11] W.L. Griffin, S.Y. O'Reilly, C.G. Ryan and M.A. Waldman, ibid.

[12] S.A.E. Johansson and J.L. Campbell, PIXE, A Novel Technique for Elemental Analysis, Wiley, (1988).

[13] J.P.F. Sellschop in 'The Properties of Diamond', J.E. Field, ed., Academic, (1979) 107.

[14] L.C. Feldman, J.W. Mayer and S.T. Picraux, 'Materials Analysis by Ion Channeling', Academic, (1982).

[15] D.N. Jamieson, R.A. Brown, C.G. Ryan and J.S. Williams, Nucl. Instr. Meth. B54 (1991) 213–224.

[16] L.T. Romano, M.B.H. Breese, D.N. Jamieson, C.Chen, G.W. Grime and F. Watt, Phy. Rev B, 44 (1991) 6927.

[17] J.M. Ballantyne and J.N. Moore, Geochim. Cosmochimi. Acta 52 (1988) 475.

[18] W.L. Griffin, P.M. Ashley, C.G. Ryan, S.H. Sie and G.F. Suter, Canadian Mineralogist, 29 (1991) 185.

[19] G.E. Jean and M. Bancroft, Geochim. Cosmoschimi. Acta 49 (1985) 979.

[20] A. Starling, J.M. Gilligan, A.H.C. Carter, R.P. Foster and R.A. Saunders, Nature, 340, (1989) 298.

[21] S.W. Knipe, R.P. Foster and C.J. Stanley, in Brazil Gold '91, *The economics, geology, geochemistry and genesis of gold deposits*, E.A. Ladeira (ed.) (1991), A.A. Balkema, Rotterdam.

[22] E.S. Dana, W.E. Ford, *A Textbook of Mineralogy*, John Wiley, 1949.

[23] M. Ahmad, M. Solomon and J.L. Walshie, Economic Geology 82 (1987) 345.

[24] W.L. Griffin, private communication, 1990.

[25] The χ_{min} and $\psi_{\frac{1}{2}}$ channeling parameters were calculated with an assumed Debye temperature of 500 K for pyrite by R.A. Brown, private communication, (1992).

[26] L.A. Clark, Econ. Geol. 55 (1960) 1345.

[27] M.E. Fleet, P.J. MacLean and J. Barbier, in *The Geology of Gold Deposits: The perspective of 1988*, R.R. Keays, W.R.H. Ramsay and D.I. Groves, eds, Econ. Geol. Monogr. 6 (1989) 356.

[28] T.M. Seward, ibid, 398.

[29] G.M. Bancroft and M.M. Hyland, in *Mineral–water interface geochemistry*, M. Hochella and A. White, eds., Min. Soc. America, Reviews in Mineralogy, 23 (1990) 511.

[30] C.G. Ryan and D.N. Jamieson, these proceedings.

[31] L.R. Doolittle, Nucl. Instr. Meth. B9 (1985) 344.

FIGURE CAPTIONS

Figure 1: Spectra obtained with the <100> axis of a cubic pyrite crystal aligned and randomly oriented to a 2 MeV He^+ beam. The large Fe 'surface peak' in the spectrum from the randomly oriented sample is due to a Fe mineral inclusion. The smooth curve is a simulation for FeS_2 from RUMP [31].

Figure 2: Angular scans through the <100> axis. Clockwise from top left: for 2 MeV He^+ for BS from Fe and S on the surface, BS from Fe (0.3 μm deep), PIXE Fe and S K_α x-ray lines (from 0.72 and 0.67 μm mean production depths respectively), angular scans for 3 MeV H^+ for PIXE Fe and Ni K_α x-ray lines (from 8.0 and 5.1 μm mean production depths respectively) and BS from Fe and S scattering from the surface. A surface barrier detector at a scattering angle of 154° was used for these measurements.

Figure 3: CCM images of a 1×1 mm square region of the 1 cm pyrite cube. The images were obtained with a 2 MeV He^+ beam and are (from left to right): the whole backscattering spectrum, Fe K_α, S K_α, Ca K_α and Si K_α.
Top row designated A: CCM images for the <100> axis aligned with the analysis beam. Light regions correspond to a low yield. Dark regions correspond to high yield, mainly from misaligned or amorphous material.
Bottom row designated R: An almost completely overlapping region of the same region covered by the top row maps with the crystal randomly oriented to the analysis beam. Light regions correspond to a low yield, mainly from inclusions.

Figure 4: Spectra from a (111) face of a truncated octohedral pyrite crystal with the <111> axis aligned and randomly oriented to a 2 MeV He^+ analysis beam.

Figure 5: BS image of a pyritohedral pyrite crystal showing a quasi-pentagonal face. The normal to the face, the <210> axis, was randomly oriented to the 2 MeV He^+ analysis beam.

Figure 6: BS spectra obtained from the centre of the pyritohedral pyrite crystal n figure 5 with the <210> axis aligned and randomly oriented to a 2 MeV He^+ analysis beam. The simulation (smooth curve) was for a nominal composition $Fe_1S_{2.4}As_{0.4}Au_{0.04}$. See text for further details.

TABLES

Table 1: Channeling results on <100> pyrite.

	2 MeV He^+			3 MeV H^+		
Feature	χ_{min} (%)	$\psi_{\frac{1}{2}}$ (°)	depth (μm)	χ_{min} (%)	$\psi_{\frac{1}{2}}$ (°)	depth (μm)
Calculated (BS) [25]	3.80	1.10	0			
S surface (BS)	3.70	1.02	0.04	10.1	0.498	0.56
Fe surface (BS)	3.70	1.46	0.05	4.16	0.767	0.82
Fe deep (BS)	6.50	1.19	0.28	-	-	-
S K_α (PIXE)	10.7	0.85	0.67	-	-	-
Ni K_α (PIXE)	-	-	-	36.3	0.484	5.12
Fe K_α (PIXE)	8.50	1.07	0.72	42.2	0.480	7.96

Table 2: Channeling results on <111> pyrite.

	2 MeV He^+	
Feature	χ_{min} (%)	depth (μm)
Calculated (BS) [25]	3.3	0
S surface (BS)	4.1	0.04
Fe surface (BS)	2.4	0.05
Fe deep (BS)	6.1	0.28
S K_α (PIXE)	20.4	0.67
Fe K_α (PIXE)	17.9	0.72

Table 3: Channeling results on <210> pyrite.

	2 MeV He^+	
Feature	χ_{min} (%)	depth (μm)
Calculated (BS) [25]	9.0	0
S surface (BS)	35	0.04
Fe surface (BS)	24	0.05
As surface (BS)	50	0.05
Au surface (BS)	50	0.05
S K_α (PIXE)	81	0.67
Au L_α (PIXE)	100	0.69
As K_α (PIXE)	94	0.70
Fe K_α (PIXE)	89	0.72

Figure 1:
D.N. Jamieson and C.G. Ryan, Microprobe Channeling Analysis of Geological Crystals.

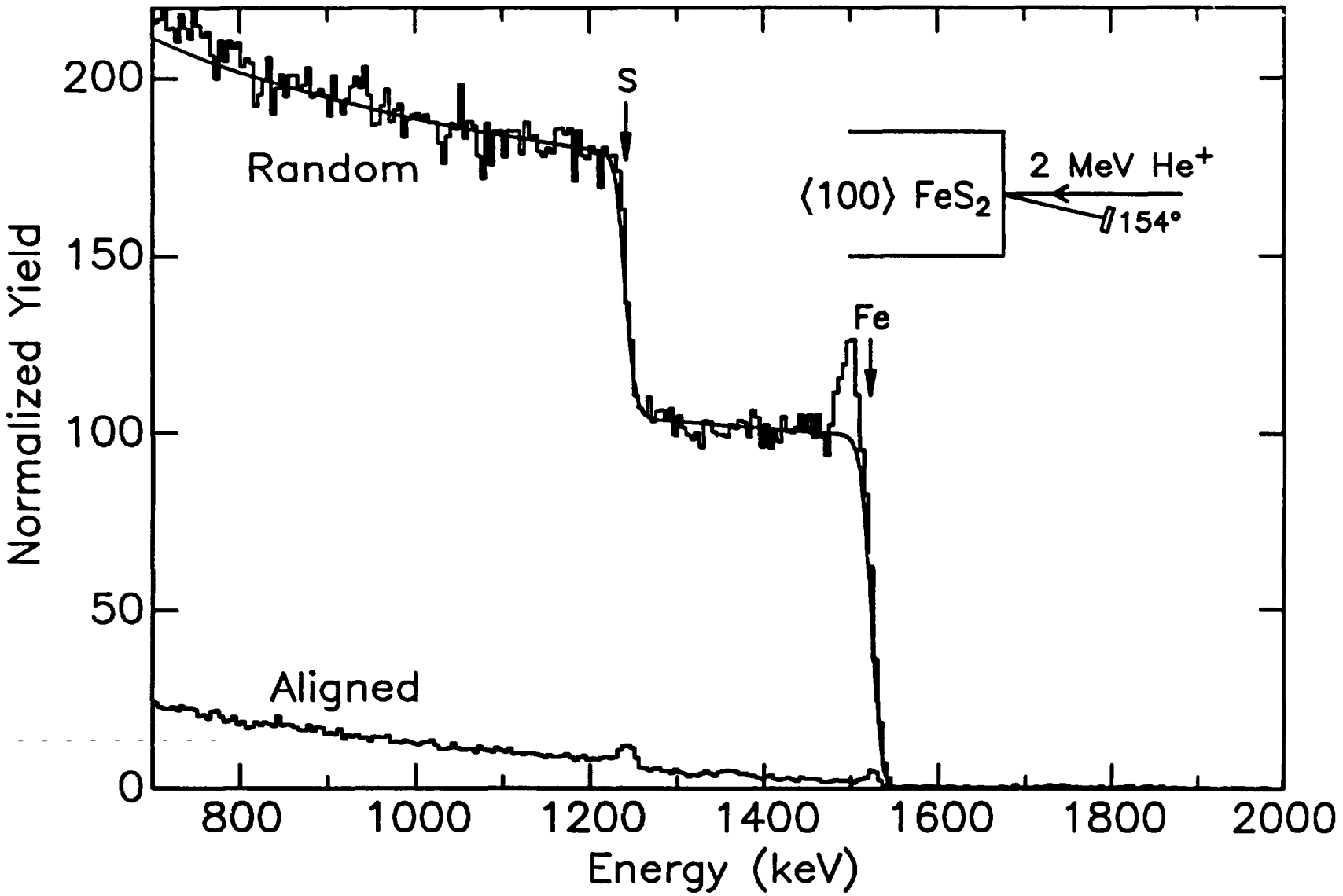

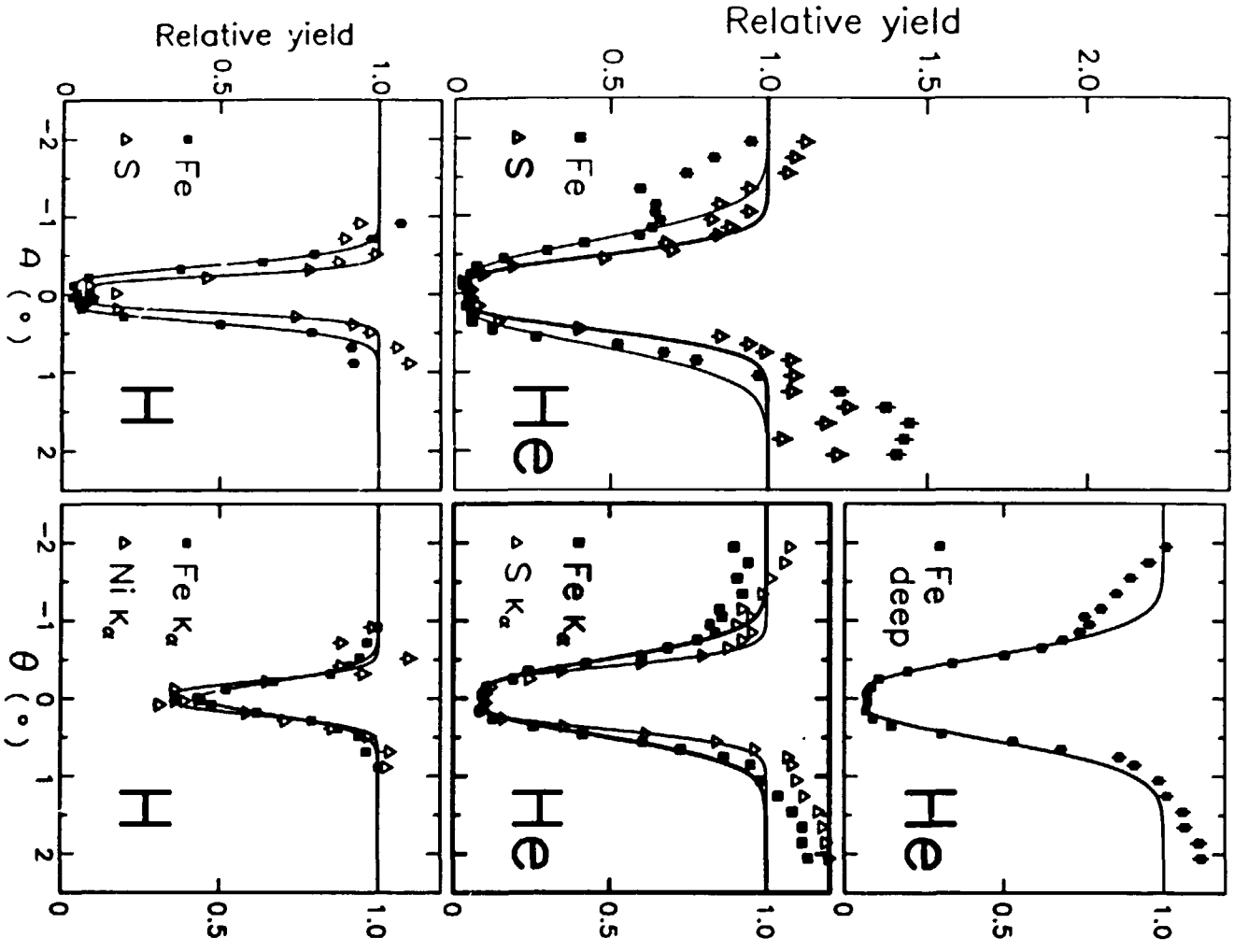

Figure 2:
D.N. Jamieson and C.G. Ryan, Microprobe Channeling Analysis of Geological Crystals.

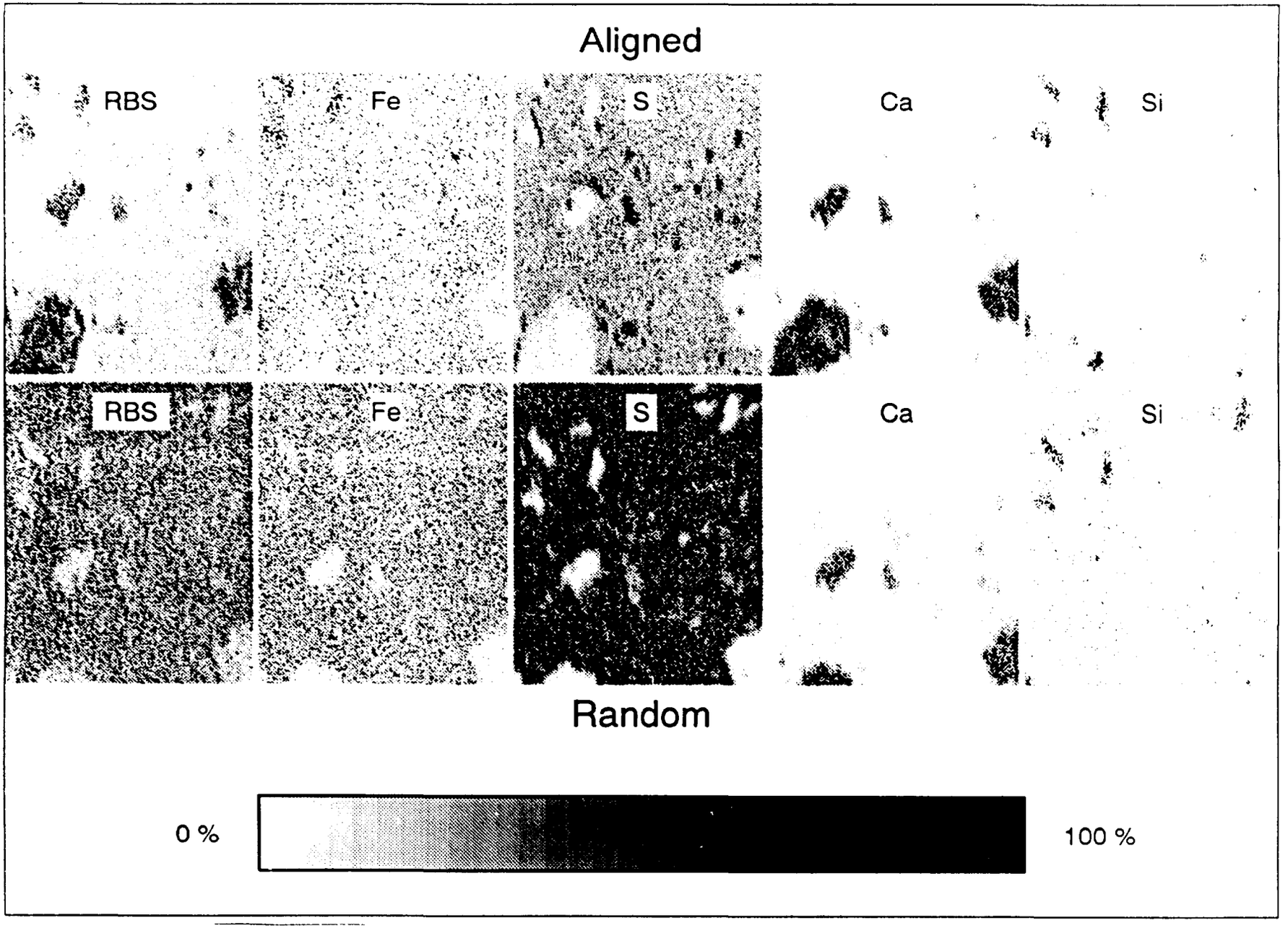

Figure 3:
D.N. Jamieson and C.G. Ryan, Microprobe Channeling Analysis of Geological Crystals.

Figure 4:
D.N. Jamieson and C.G. Ryan, Microprobe Channeling Analysis of Geological Crystals.

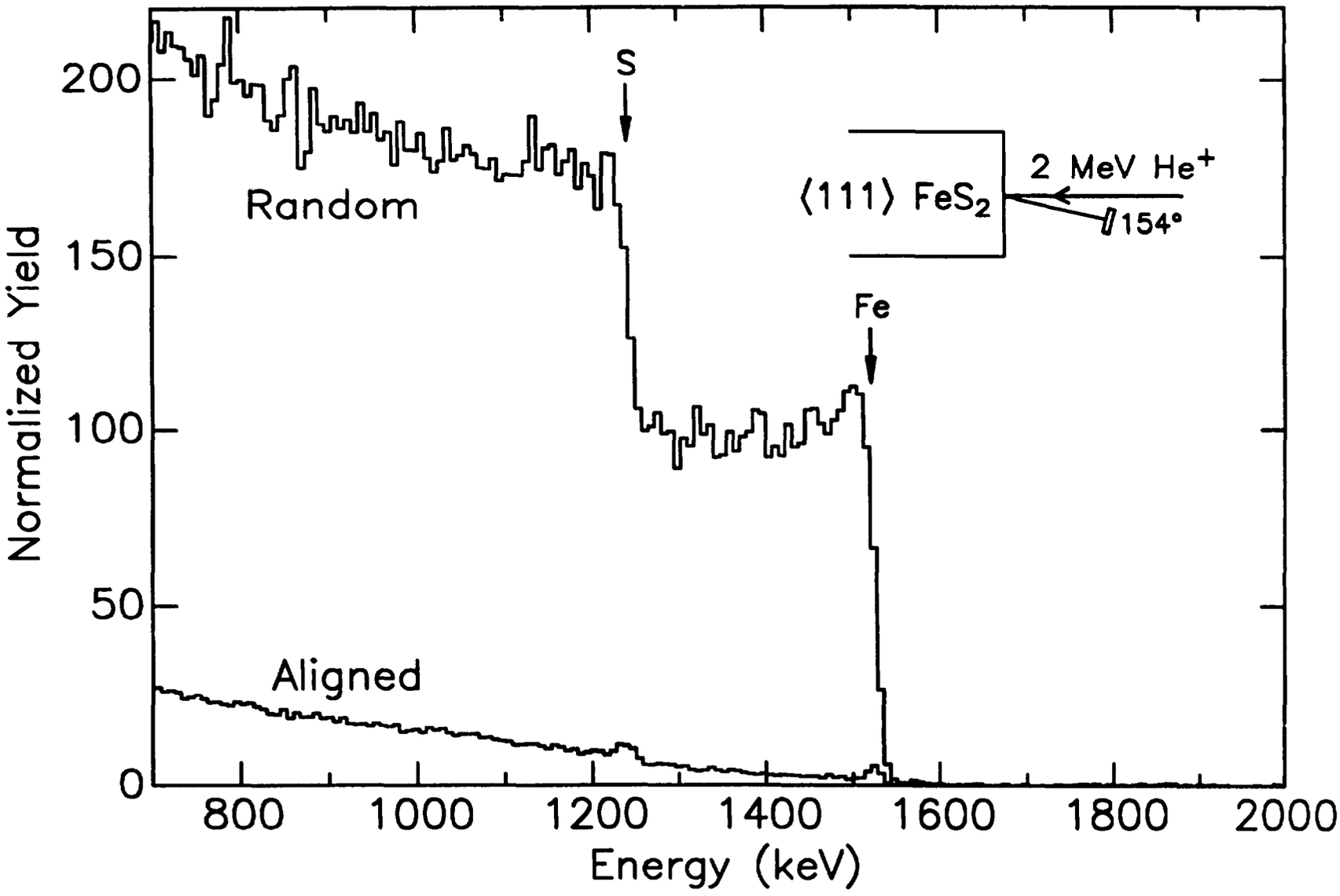

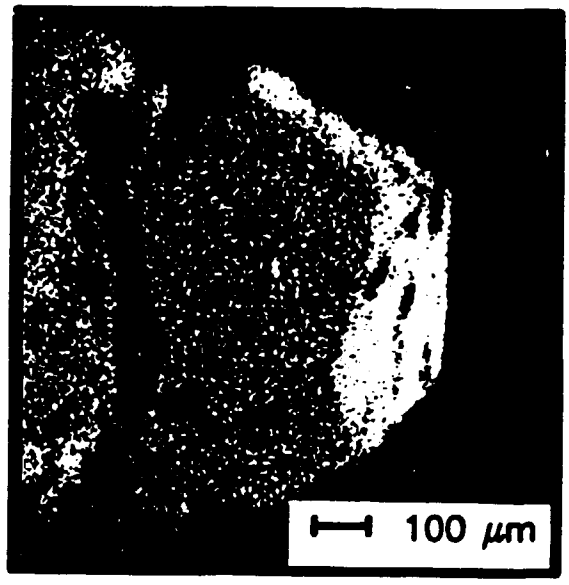

Figure 5:
D.N. Jamieson and C.G. Ryan, Microprobe Channeling Analysis of Geological Crystals.

Figure 6:
D.N. Jamieson and C.G. Ryan, Microprobe Channeling Analysis of Geological Crystals.